Double pendulum: An experiment in chaos

R. B. Levien
Department of Physics, Princeton University, Princeton, New Jersey 08544

S. M. Tan
Department of Physics, University of Auckland, Auckland, New Zealand

(Received 10 December 1992; accepted 1 April 1993)

We describe an experiment which takes advantage of the surprising complexity of one of the simplest physical systems, the passive double pendulum. For large angle swings sensitive dependence on initial conditions, the signature of chaos, may be demonstrated and quantified in a very direct way. Small angle experiments and zero gravity experiments (with the pendulum swinging in a horizontal plane) may also be performed. The angles are measured very precisely and reliably using optical encoder wheels, and data are acquired and displayed using a personal computer. The experiment is suitable for the undergraduate laboratory.

I. INTRODUCTION

In recent years there have been many experimental demonstrations of chaotic motion, including some suitable for the undergraduate laboratory.[1–8] Most of these involve driven systems; they have the advantage that they may be observed over long time periods, which is essential for constructing Poincaré plots. However, a disadvantage of a driven system is that it is often difficult to control the initial conditions precisely, as the state of both the driving system and the system proper must be controlled simultaneously. The real beauty of the passive double pendulum system is that the defining characteristic of chaos, namely sensitive dependence on initial conditions, may be convincingly demonstrated simply by performing the experiment twice with starting conditions which match very closely [see Fig. 8(b)]; an initial separation of less than 1° is magnified over 1000-fold in a matter of seconds. This makes the system ideal for lecture demonstrations of chaos. We can measure the rate of divergence of nearby trajectories, and compare this with numerically calculated Lyapunov exponents (defined in Sec. II below).

A second advantage is the flexibility of the system. As well as the chaotic large angle motion, the small angle motion, for which the equations of motion are approximately linear, provides a good illustration of normal modes. And we can study zero gravity motion (i.e., no restoring torque) by tilting the whole apparatus through 90°, so that the pendulum swings in the horizontal plane.

The two angles are measured using Hewlett–Packard optical encoder wheels, as in the simple driven pendulum experiment of Blackburn *et al.*[3] To couple information out from the lower pendulum, we use a small AM transmitter mounted on the outer pendulum, and a receiver mounted on the pendulum frame. The data are acquired by an MS-DOS 386 PC and manipulated and plotted using MatLab.

While writing this we became aware of a recently published double pendulum experiment,[9] that also looks at the divergence of nearby trajectories. The clear advantage of our experiment is that the angles are measured in real time, and the data are acquired and displayed on a PC, eliminating the need for the time-consuming analysis of photographs of stroboscopic trajectories. A typical large angle experiment involving 10 runs takes a matter of minutes, and it was our aim to have the small angle, zero gravity, and large angle experiments all completable in a 3 h undergraduate laboratory session.

II. THEORY

For the moment we make the idealization of no damping, and treat the double pendulum as a Hamiltonian system. This assumption is good provided we keep the runs short enough that the energy damping is only a few percent; we return to this point in Sec. IV. The Lagrangian for an undamped double pendulum free to move in a plane is given by

$$\mathcal{L}=T-V, \tag{1}$$

where the kinetic energy T and the potential energy V are

$$T=\tfrac{1}{2}(I_1+m_2l_3^2)\dot{\phi}_1^2+\tfrac{1}{2}I_2(\dot{\phi}_1+\dot{\phi}_2)^2+m_2l_2l_3\dot{\phi}_1(\dot{\phi}_1+\dot{\phi}_2)\cos\phi_2, \tag{2}$$

$$V=g(m_1l_1+m_2l_3)(1-\cos\phi_1)+m_2gl_2[1-\cos(\phi_1+\phi_2)], \tag{3}$$

where g is the gravitational acceleration. ϕ_1 and ϕ_2 are the angles associated with pendulums 1 and 2, respectively (see Fig. 1). $\dot{\phi}_i=d\phi_i/dt$. Note that ϕ_1 is measured from the vertical, while ϕ_2 is measured from the line joining the two pivot points. We will refer to pendulum 1 as the "outer" pendulum and pendulum 2 as the "inner" pendulum, because this was the way in which our apparatus was constructed (see Fig. 4). m_1 and m_2 are the masses of the outer pendulum and the inner pendulum respectively, and l_1 and l_2 are the displacements of the center of mass from their respective pivot points (see Fig. 1). l_3 is the distance between the two pivot points, and I_1 and I_2 are the moments of inertia of the two pendula about their respective pivots. We note that because of the complicated shape of the real pendula (see Fig. 4) the moments of inertia I_i would be awkward to calculate in terms of m_i and l_i; but they are easily measured directly, as we describe in Sec. III. The momenta conjugate to ϕ_1 and ϕ_2 are

$$L_1=\frac{\partial\mathcal{L}}{\partial\dot{\phi}_1}=\dot{\phi}_1(I_1+m_2l_3^2+I_2+2m_2l_2l_3\cos\phi_2)+\dot{\phi}_2(I_2+m_2l_2l_3\cos\phi_2), \tag{4}$$

© 1993 American Association of Physics Teachers

$$L_2=\frac{\partial \mathcal{L}}{\partial \dot{\phi}_2}=\dot{\phi}_1(I_2+m_2 l_2 l_3 \cos\phi_2)+\dot{\phi}_2 I_2. \tag{5}$$

L_1 is just the total angular momentum of the system about the pivot point of the outer pendulum, while L_2 does not have such a simple interpretation. From these we may write down the Euler–Lagrange equations governing the motion of the system

$$\frac{d}{dt}\left(\frac{\partial \mathcal{L}}{\partial \dot{\phi}_i}\right)=\frac{\partial \mathcal{L}}{\partial \phi_i}, \tag{6}$$

and solve these equations for $\ddot{\phi}_1$ and $\ddot{\phi}_2$. The variables ϕ_1, ϕ_2, $\dot{\phi}_1$, $\dot{\phi}_2$ (the two angles and corresponding angular velocities) then define a four-dimensional phase space.

We may also use the Hamiltonian formulation, in which case we find

$$H=\sum_{i=1,2} L_i\dot{\phi}_i-\mathcal{L} \tag{7}$$

$$=\frac{L_1^2 I_2+L_2^2(I_1+m_2 l_3^2+I_2+2m_2 l_2 l_3\cos\phi_2)-2L_1L_2(I_2+m_2 l_2 l_3\cos\phi_2)}{2I_2(I_1+m_2 l_3^2)-2m_2^2 l_2^2 l_3^2\cos^2\phi_2}+g(m_1 l_1+m_2 l_3)(1-\cos\phi_1)$$

$$+m_2 g l_2[1-\cos(\phi_1+\phi_2)]. \tag{8}$$

With no damping, we have

$$H=T+V=E, \tag{9}$$

where the total energy E is conserved; the system is then referred to as a "Hamiltonian system." Hamilton's equations of motion are given by

$$\dot{\phi}_i=\frac{\partial H}{\partial L_i}, \tag{10}$$

$$\dot{L}_i=-\frac{\partial H}{\partial \phi_i}; \tag{11}$$

the four variables in our phase space are then (ϕ_1,ϕ_2,L_1,L_2).

For small angle motion, or if g is zero, the system is integrable; that is, there is another conserved quantity besides the energy. These cases are presented below. But for nonzero g and large angles of swing, we have a nonintegrable Hamiltonian system, which displays a rich range of dynamics, including chaos. The most detailed treatments we have found are by Rott,[10] who makes the approximation of quadratic coupling and Richter and Scholtz,[11] who present a series of Poincaré sections to illustrate the incredible richness and beauty of the dynamics.

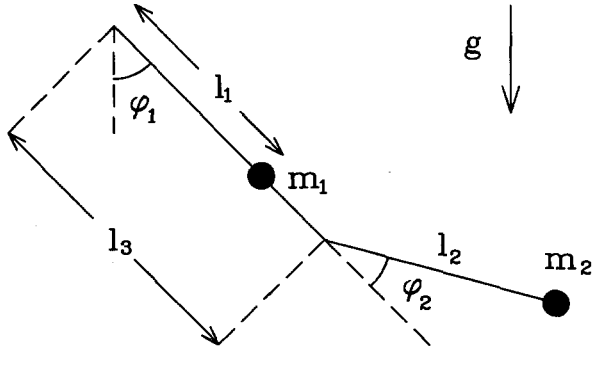

Fig. 1. The double pendulum. m_1 and m_2 are the masses of each pendulum; the dots represent the center of mass positions.

A. Small angle motion

For small angles ϕ_1,ϕ_2 we can linearize the Lagrange Eqs. (6) to obtain

$$\begin{pmatrix}\ddot{\phi}_1\\ \ddot{\phi}_2\end{pmatrix}=\frac{1}{d}\begin{pmatrix}c_1 & c_2\\ c_3 & c_4\end{pmatrix}\begin{pmatrix}\phi_1\\ \phi_2\end{pmatrix}, \tag{12}$$

where

$$c_1=m_2^2 g l_2^2 l_3-I_2 g(m_1 l_1+m_2 l_3), \tag{13}$$

$$c_2=m_2^2 g l_2^2 l_3, \tag{14}$$

$$c_3=I_2 g(m_1 l_1+m_2 l_3)+m_2 g l_2(m_1 l_1 l_3-I_1-m_2 l_2 l_3), \tag{15}$$

$$c_4=-m_2 g l_2(m_2 l_2 l_3+m_2 l_3^2+I_1), \tag{16}$$

$$d=I_2(I_1+m_2 l_3^2)-m_2^2 l_2^2 l_3^2. \tag{17}$$

Because the equations are now linear, the motion is regular, and easily analyzed. There are two normal modes, with frequencies

$$\omega_{1,2}^2=\frac{-(c_1+c_4)\pm\sqrt{(c_1+c_4)^2-4(c_1c_4-c_2c_3)}}{2d}. \tag{18}$$

The corresponding eigenvectors have

$$\frac{\phi_2}{\phi_1}=\frac{c_4-c_1\mp\sqrt{(c_1+c_4)^2-4(c_1c_4-c_2c_3)}}{2c_2}. \tag{19}$$

We could now rewrite an arbitrary small angle motion as a sum of the two normal modes.[12] The amplitude of each normal mode component is a constant of the motion, so this is an integrable limit.

B. Zero gravity motion

If we tilt the pendulum on its side there is no restoring torque due to gravity, so that $g=0$ as far as the pendulum is concerned. From Eqs. (8)–(11) we can show (see Ref. 11) that the total angular momentum L_1 is conserved (i.e., we have another integrable limit), and that

$$\dot{\phi}_2 = \pm \sqrt{\frac{2E(I_1 + m_2 l_3^2 + I_2 + 2m_2 l_2 l_3 \cos\phi_2) - L_1^2}{I_2(I_1 + m_2 l_3^2) - m_2^2 l_2^2 l_3^2 \cos^2\phi_2}}. \quad (20)$$

We may deduce from Eq. (20) that for a given energy E there is a maximum value of L_1. Defining

$$l_1 \equiv \frac{L_1}{\sqrt{E}} \quad (21)$$

we obtain the result

$$l_1^{\max} = \sqrt{2(I_1 + I_2 + m_2 l_3^2 + 2m_2 l_2 l_3)}, \quad (22)$$

which occurs when $\phi_2 = 0$ (i.e., the pendulum is stretched out). We can also see that $\dot{\phi}_2$ cannot be zero if $|l_1| < l_1^{\text{sep}}$, where

$$l_1^{\text{sep}} = \sqrt{2(I_1 + I_2 + m_2 l_3^2 - 2m_2 l_2 l_3)}. \quad (23)$$

This means that the lower pendulum rotates ($\dot{\phi}_2$ never changes sign). However for $|l_1| > l_1^{\text{sep}}$, the lower pendulum oscillates, with $|\phi_2| < \pi$.

C. Large angle motion

For large angles of swing and nonzero gravity the motion of the pendulum is nonintegrable and often chaotic. A definition of chaos is that nearby trajectories in phase space tend to diverge exponentially in time. If we have two nearby starting points $\phi_i^I(0)$ and $\phi_i^{II}(0)$, then as we let the system evolve,

$$|\phi_i^{II}(t) - \phi_i^I(t)| \sim e^{\lambda t}. \quad (24)$$

The average rate λ of divergence or convergence is called a Lyapunov exponent. In n-dimensional phase space there are n Lyapunov exponents $\lambda_{i=1,\ldots,n}$, which describe what happens to a small sphere of initial points.[13] We order the exponents so that λ_1 is the largest exponent and λ_n the smallest. The sphere is stretched into an ellipsoid, the n Lyapunov exponents describing the contraction or expansion of the ellipsoid along its principal axes.

If at least one Lyapunov exponent is positive, the system is chaotic; even if the starting conditions are known very precisely, any small error is rapidly magnified in time, and predictive power is lost.

We numerically calculated the Lyapunov exponents using an algorithm[14–16] which numerically integrates both the n nonlinear equations of motion, and n copies of the linearized equations (which describe the evolution of small displacements about the current point in phase space). The initial conditions for the linearized equations are a set of n orthonormal vectors. Thus we are investigating a set of deviations about the current point. As time goes on all these vectors tend to diverge in magnitude, and they tend to point in the direction of most rapid growth. A Gram–Schmidt orthonormalization is carried out on the displacement vectors every few time steps. The result of this procedure is that the first vector tends to grow as $e^{\lambda_1 t}$, the area defined by the first two vectors tends to grow as $e^{(\lambda_1+\lambda_2)t}$, and so on. In this way all n Lyapunov exponents may be calculated (see Ref. 14 for a more detailed description of the algorithm).

Figure 2 shows such a calculation, for the system parameters given in Eq. (25) below, and initial conditions $\phi_1(0) = -\phi_2(0) = 120°$, $\dot{\phi}_1(0) = \dot{\phi}_2(0) = 0$ (i.e., the outer pendulum displaced through 120° from the vertical, and the inner pendulum hanging straight down). We note the exponents converging as they are averaged over time. Note also that the four exponents sum to zero, as indeed they must by Liouville's theorem,[12] which tells us that the size of a small volume element in phase space does not change with time, for a conservative system. Repeating this process for a range of different starting angles ϕ_1 (but always with the second pendulum just hanging, and both pendula at rest), we obtain. Fig. 3, which shows the dominant (most positive) Lyapunov exponent as a function of the starting angle.

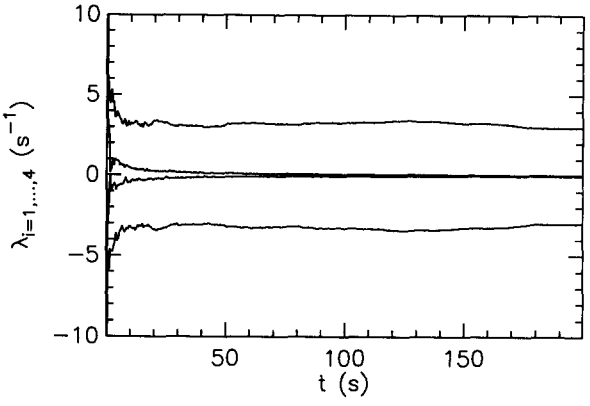

Fig. 2. Numerical calculation of the four Lyapunov exponents for $\phi_1(0) = -\phi_2(0) = 120°$, $\dot{\phi}_1(0) = \dot{\phi}_2(0) = 0$.

III. APPARATUS

The double pendulum itself (see Fig. 4) is made from aluminium, with four hardened steel pivot bearings (each consisting of a single cone resting in a conical recess of a greater opening angle, so that each pendulum is supported at just two points) to minimize bearing friction. The system parameters were (see Fig. 1)

$$\begin{aligned} &g = 9.799\,403 \text{ m s}^{-2}, \quad m_1 = 261.9 \text{ g}, \quad m_2 = 87.7 \text{ g}, \\ &l_1 = 20 \times 10^{-3} \text{ m}, \quad l_2 = 25 \times 10^{-3} \text{ m}, \\ &l_3 = 57 \times 10^{-3} \text{ m}, \quad I_1 = 6.43 \times 10^{-4} \text{ kg m}^2, \\ &I_2 = 7.86 \times 10^{-5} \text{ kg m}^2. \end{aligned} \quad (25)$$

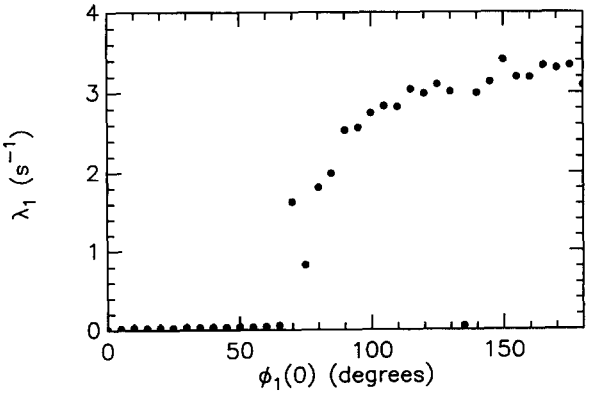

Fig. 3. Numerical calculation of the most positive Lyapunov exponent for different initial conditions $\phi_1(0)$. In all cases $\phi_2(0) = -\phi_1(0)$, and $\dot{\phi}_1(0) = \dot{\phi}_2(0) = 0$.

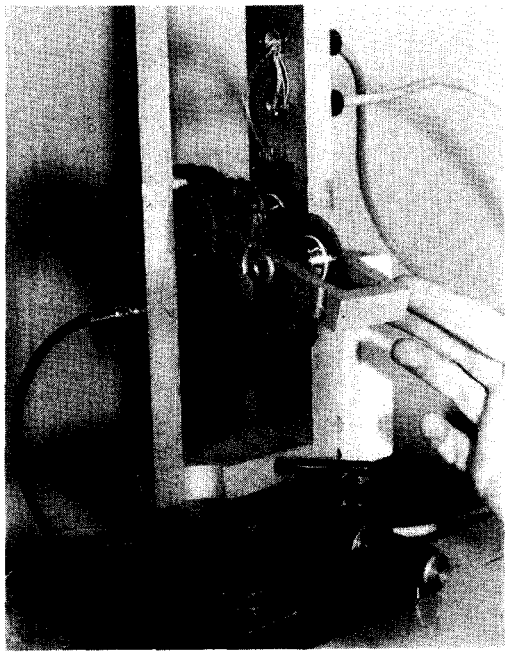

Fig. 4. The double pendulum apparatus.

l_1 and l_2 (the positions of the centers of mass for each pendulum) were measured by balancing each pendulum individually on a length of thread; I_1 and I_2 (the moments of inertia of each pendulum about its pivot point) were measured dynamically, by timing small angle swings for each pendulum in turn, which have period

$$T_i = 2\pi\sqrt{\frac{I_i}{mgl_i}}. \tag{26}$$

Each of the angles ϕ_1, ϕ_2 is measured using a HP model HEDS-6100 code wheel and a HP model HEDS-9000 encoder module.[3] The encoder is a C-shaped module with a single lensed light-emitting diode (LED) on one side of a 1.8 mm gap, and four photodetectors on the other. The code wheel, a 5 cm diam metal foil disk, rotates between the LED and the detectors. 1000 slots are cut into the periphery of the disk in such a way that when two detectors are illuminated, the adjacent pair are in darkness. There are two channels of transistor–transistor-logic (TTL)-compatible output, consisting of two square waves 90° out of phase. Thus there are four distinct binary patterns corresponding to the passage of a single slot; so the angle is measured to 360/4000 = 0.09° accuracy, and direction is sensed as well.

For angle ϕ_1 the output of the encoder is fed directly to a HP model HCTL-2000 12 bit counter on a prototype board (a PR-2 from JDR Microdevices) in the PC (a MS-DOS 386). To measure angle ϕ_2 we did not want to use wires (which would twist) or brushes (which would introduce extra friction) to couple the information out, so an alternative had to be found. ϕ_2 is measured with an encoder, and the two output channels are amplitude modulated up to 8 and 10 MHz using two ceramic resonators and a 7400 NAND gate mounted on the outer pendulum (see Fig. 5). The 5 V power supply for the encoder module and the NAND gate is provided by a 9 V battery and a 78L05 regulator, mounted on the outer pendulum (see Fig. 4). The output of the NAND gate drives a small transmitting coil mounted on the outer pendulum, which is inductively coupled to a receiving coil mounted on the frame. Both coils are mounted on the pivot axis, so the geometry remains the same as the outer pendulum is rotated. The signal from the receiving coil is fed via a coaxial cable to a box mounted on the pendulum frame, where it is amplified using a NE 592 broadband video amplifier (see Fig. 5). Two more of these amplifiers separate out the 8 and 10 MHz components using the same type of ceramic resonators; then rectification and low-pass filtering stages and a TTL-compatible comparator (LM 339) reconstructs the

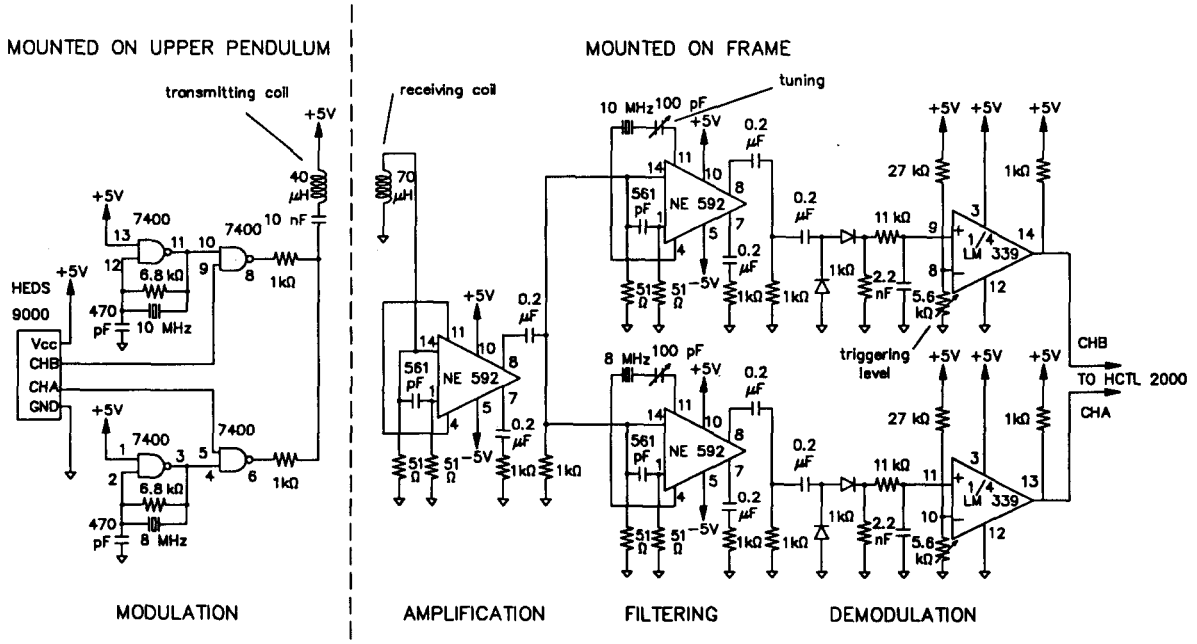

Fig. 5. The modulation/demodulation circuit.

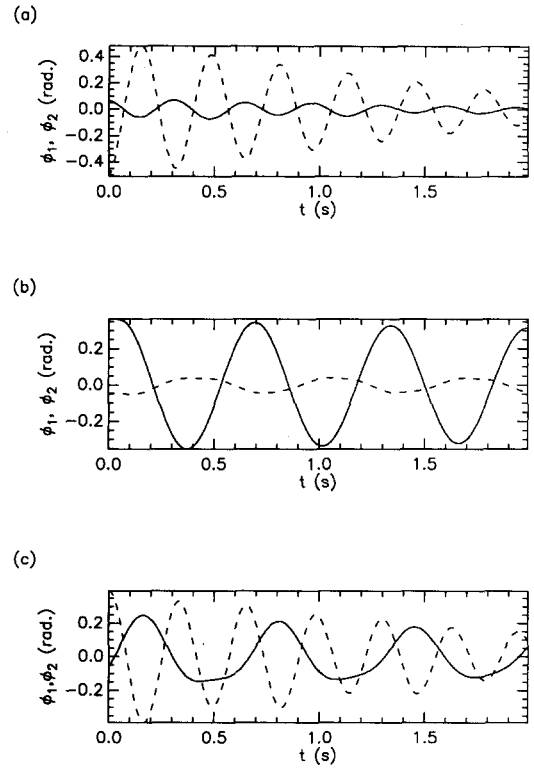

Fig. 6. Small angle results. The solid lines are $\phi_1(t)$, the dotted lines are $\phi_2(t)$. Graph (a) shows the high frequency normal mode, graph (b) the low frequency normal mode, and graph (c) a sum of the two modes.

square wave signals. The output of the LM 339 is then fed to another HCTL-2000 on the prototype board.

The HCTL-2000 is a 12 bit counter, but the high byte and the low byte must be read separately, via an 8 bit output port. The output ports of the two HCTL-2000's are connected to ports A and B of an INTEL 8255 Programmable Peripheral Interface chip, in mode 0 (basic input/output). Two further 4 bit ports on the 8255 are used to control the HCTL-2000's. An INTEL 8254 timer chip in mode 3 (square wave mode), with sampling frequency set by the user, generates an interrupt signal every sampling period, whereupon the PC reads the current count from both HCTL-2000's. The time interval between samples varied between 1 ms and 0.1 s.

IV. EXPERIMENTAL RESULTS

A. Small angle motion

The small angle motion is shown in Fig. 6, which shows experimental data. The solid lines show $\phi_1(t)$, and the dotted lines $\phi_2(t)$. Graph (a) shows the high frequency mode, graph (b) the low frequency mode, and graph (c) an arbitrary sum of the two. To excite each normal mode we made use of Eq. (19) and the parameters given in Eq. (25) to find the corresponding eigenvector. The angles ϕ_1 and ϕ_2 are displayed in real time on the computer screen until a key is hit to begin recording data; so with a little dexterity the user can set the two initial angles. The fact that the user can manually adjust the start vector to be an eigenvector makes this a good "hands-on" illustration of normal modes. The time between samples was set at 1 ms, so the period of the normal mode oscillations could be precisely determined by simply measuring the time between zero

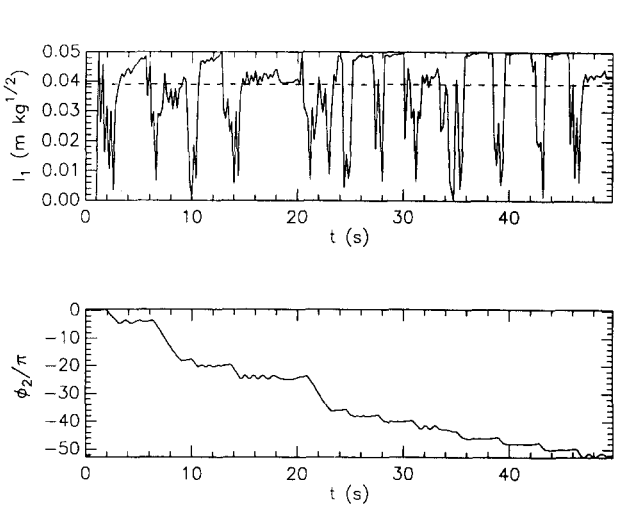

Fig. 7. Zero gravity results. Graph (a) shows l_1 as a function of time (solid line) and l_1^{sep} (dotted line). Graph (b) shows $\phi_2(t)$.

crossings (the pendulum is "zeroed" by letting it hang before the start of each run). We obtained normal mode frequencies

$$f_1 = 3.06 \pm 0.06 (3.14 \pm 0.01) \text{ Hz}, \tag{27}$$

$$f_2 = 1.55 \pm 0.02 (1.566 \pm 0.005) \text{ Hz}, \tag{28}$$

where the theoretical values [from Eq. (18)] are shown in brackets. For the error in the measured values we have simply taken the difference between the frequencies measured using the ϕ_1 and ϕ_2 data. This is a measure of how precisely we have excited each normal mode [compare Fig. 6(c) to Figs. 6(a) and 6(b)].

B. Zero gravity motion

Figure 7 shows the results of the zero gravity experiment. The graph requires some explanation. We wished to illustrate the change from ϕ_2 rotation to ϕ_2 oscillation, depending on the value of

$$l_1 = \frac{L_1}{\sqrt{E}}. \tag{29}$$

To do this, we set the inner pendulum rotating [this corresponds to the times when graph 7(b) is monotonically decreasing], then give the outer pendulum a push, aiming to change the value of l_1. If l_1 is now greater than l_1^{sep}, we expect the ϕ_2 motion (of the inner pendulum) to become oscillation. We then stop the pendulum and repeat the experiment many times; thus Fig. 7 actually shows several repetitions of this procedure. The value of $l_1^{sep} = 0.039$ m kg$^{1/2}$ is shown in the dotted line in Fig. 7(a). We expect l_1 to be piecewise constant in time; the oscillations seen in graph 7(a) are due to small errors in the parameter values in Eq. (25). The theoretical limit on l_1 is $l_1^{max} = 0.050$ m kg$^{1/2}$. For $0 < l_1 < l_1^{sep}$ we see ϕ_2 rotation, and for $l_1^{sep} < l_1 < l_1^{max}$ we see ϕ_2 oscillation.

To calculate L_1 and E we needed the angular velocities, $\dot{\phi}_1(t)$ and $\dot{\phi}_2(t)$, which we calculated from the time series $\phi_1(t)$ and $\phi_2(t)$, using a least squares fit to the last few points, with an exponentially decreasing weight.

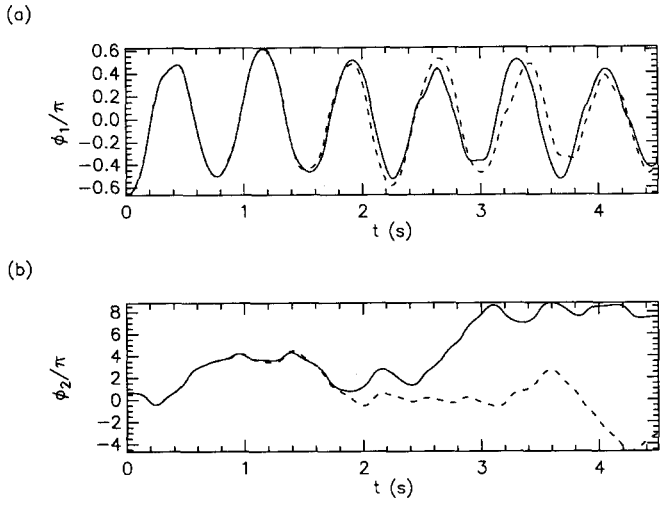

Fig. 8. Large angle results. Graph (a) shows $\phi_1(t)$, graph (b) shows $\phi_2(t)$; the solid and dotted lines are two runs with very similar initial conditions.

C. Large angle motion

Figure 8 shows two runs with initial conditions $\phi_1(0) = -\phi_2(0) \simeq -120°$, $\dot{\phi}_1(0) = \dot{\phi}_2(0) = 0$ (as for the small angle experiment, the angles are displayed in real time on the computer screen, so the initial angles may be set quite precisely). To overlay the plots, we started collecting data before letting the pendula go, then chopped off the zero velocity part at the beginning of each run. The sensitive dependence on initial conditions is dramatically illustrated, as an initial difference in $\phi_2(0)$ of less than 1° is amplified by three orders of magnitude in less than 5 s. The divergence is completely dominated by the largest Lyapunov exponent λ_1, so this is by far the easiest exponent to measure experimentally. The other exponents may in principle be extracted from the experimental data, but the analysis is far more complex [see Ref. 14] and longer runs are needed, whereupon damping becomes much more of a problem (see below).

To quantify this divergence rate, we took ten 5 s runs with as near as possible to the same starting conditions. We then estimated the rate of divergence by taking the ϕ_2 trajectories $\phi_2^i(t)$ $(i=1,...,10)$, and making a linear fit to the log of the difference between all pairs of trajectories

$$\ln|\phi_2^i(t) - \phi_2^j(t)| \sim \lambda_1^{\text{est}} t. \tag{30}$$

We note that there is nothing special about ϕ_2; we obtained the same divergence rate λ_1 using the the ϕ_1 trajectories, as all variables diverge at the same rate (we could also have used $\dot{\phi}_1$ or $\dot{\phi}_2$, but these variables are not directly measured). As the trajectories diverged in time, we used only a subset of the full data set to estimate λ_1^{est}. For each pair of trajectories we only used data from time $t=0$ up to the time at which the difference between the two trajectories had grown to a cutoff size, $(\Delta\phi_2)^{\max}$. We then averaged the results for all pairs of trajectories to get an average divergence rate.

Figure 9 shows the results of the calculation. We have plotted the estimated divergence rate λ_1^{est} vs the maximum difference $(\Delta\phi_2)^{\max}$ between any two trajectories that we allowed in the calculation. In actual fact the difference trajectories $\phi_2^i(t) - \phi_2^j(t)$ typically oscillated in time as well

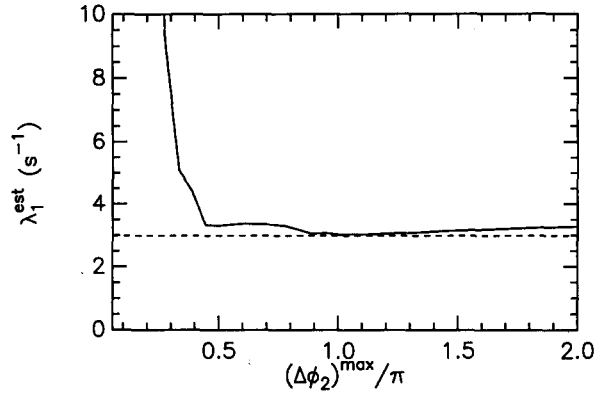

Fig. 9. Estimate of the divergence rate of nearby trajectories, as a function of the maximum separation between trajectories (solid line). The initial conditions were $\phi_1(0) = -\phi_2(0) \simeq 120°$, $\dot{\phi}_1(0) = \dot{\phi}_2(0) = 0$. The dotted line is the numerical calculation of the dominant Lyapunov exponent.

as growing exponentially, so the fit to a simple exponential was very crude. For small $(\Delta\phi_2)^{\max}$ we are looking at the oscillatory behavior, and hence obtain an inflated estimate of the divergence rate. For large $(\Delta\phi_2)^{\max}$ the trajectories are no longer "close," and so the divergence rate is no longer a sensible thing to measure. But at some intermediate range of $(\Delta\phi_2)^{\max}$, we expect the calculation to converge on the actual divergence rate, as we can see happening in Fig. 9. The dotted line shows the numerically calculated dominant Lyapunov exponent, for the same initial conditions. It should be stressed that the Lyapunov exponent is by definition an average over a long time period; while we have only measured the initial divergence rate. So while we might have expected agreement to within an order of magnitude, the fact that we get such close agreement must be reflecting a peculiarity of the system rather than a general rule.

Figure 10 shows a similar calculation for initial conditions $\phi_1(0) = -\phi_2(0) \simeq 75°$, $\dot{\phi}_1(0) = \dot{\phi}_2(0) = 0$. Again the numerically calculated dominant Lyapunov exponent is shown in the dotted line; we note that it is much greater than the actual divergence rate. Because in this case the divergence rate is much smaller (see Fig. 4), we had to take 10 s runs instead of 5 s runs. The effect of the damping then must be taken into account. We can build damping

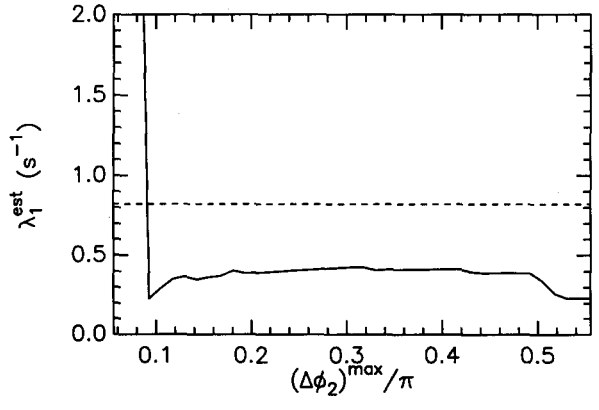

Fig. 10. Estimate of the divergence rate of nearby trajectories, for $\phi_1(0) = -\phi_2(0) \simeq 75°$, $\dot{\phi}_1(0) = \dot{\phi}_2(0) = 0$ (solid line). The dotted line is the numerically calculated dominant Lyapunov exponent.

into the equations of motion in a phenomenological way, by adding terms $-2\alpha_i\dot{\phi}_i$ to $\ddot{\phi}_i$, where $\alpha_1 \simeq 0.05\ s^{-1}$ and $\alpha_2 \simeq 0.09\ s^{-1}$, from measurements of the damping rate for each pendulum individually. When this is done and the Lyapunov exponents are numerically calculated over a 10 s time period in an attempt to duplicate the experiment, we obtain for the largest exponent $\lambda_1 = 0.41 \pm 0.04\ s^{-1}$ (the error reflects the amplitude of the fluctuations in the numerical estimation of λ_1 after 10 s; compare Fig. 3), in good agreement with the measured value.

V. CONCLUSIONS

We have described an experiment which is able to reveal some of the dynamical complexity of one of the simplest of physical systems, the double pendulum. As well as a convincing demonstration of the defining characteristic of chaos, sensitive dependence on initial conditions, experiments in the two integrable limits of small angle motion and zero gravity motion may also be performed.

The damping rate was too high to see experimentally the beautiful Poincaré plots (needing many cycles of motion with only small percentage energy loss) that have been seen in numerical calculations.[11] However, scaling the apparatus up in mass appeared to raise the effective Q of the system, (though our pivot bearings would probably have to be replaced by something more sturdy) so such an experiment may be possible in the future.

ACKNOWLEDGMENTS

We would like to thank Professor H. J. T. Smith of the Department of Physics, University of Waterloo, Waterloo, Ontario, Canada, for his very kind help with the angle measuring technology. Many thanks are also due to Eric Strickett in the machine shop for the mechanical construction of the pendulum and for helpful ideas, and to one of the referees for many constructive suggestions.

[1] K. Briggs, "Simple experiments in chaotic dynamics," Am. J. Phys. **55**, 1083–1089 (1987).

[2] Y. Cohen, S. Katz, A. Peres, E. Santo, and R. Yitzhaki, "Stroboscopic view of regular and chaotic orbits," Am. J. Phys. **56**, 1042 (1988).

[3] J. A. Blackburn, S. Vik, B. Wu, and H. J. T. Smith, "Driven pendulum for studying chaos," Rev. Sci. Instrum. **60**, 422–426 (1989).

[4] M. Ballico, M. Sawley, and F. Skiff, "The bipolar motor: A simple demonstration of deterministic chaos," Am. J. Phys. **58**, 58–61 (1990).

[5] A. Ojha, S. Moon, B. Hoeling, and P. B. Siegel, "Measurements of the transient motion of a simple nonlinear system," Am. J. Phys. **59**, 614–619 (1991).

[6] B. Duchesne, C. W. Fischer, C. G. Gray, and K. R. Jeffrey, "Chaos in the motion of an inverted pendulum: An undergraduate laboratory experiment," Am. J. Phys. **59**, 987–992 (1991).

[7] F. Moon, *Chaotic Vibrations* (Wiley, New York, 1987).

[8] N. B. Tufillaro, T. Abbott, and J. Reilly, *An Experimental Approach to Nonlinear Dynamics and Chaos* (Addison–Wesley, Redwood City, CA, 1991).

[9] T. Shinbrot, C. Grebogi, J. Wisdom, and J. A. Yorke, "Chaos in a double pendulum," Am. J. Phys. **60**, 491–499 (1992).

[10] N. Rott, "A multiple pendulum for the demonstration of nonlinear coupling," Z. Angew. Math. **21**, 570–582 (1970).

[11] P. H. Richter and H. J. Scholz, "Chaos in Classical Mechanics: The Double Pendulum," in *Stochastic Phenomena and Chaotic Behaviour in Complex Systems*, edited by P. Schuster (Springer, Berlin, 1983).

[12] H. Goldstein, *Classical Mechanics*, 2nd ed. (Addison–Wesley, Reading, MA, 1980), pp. 253–258 (normal modes), pp. 426–428 (Liouville's theorem).

[13] G. L. Baker and J. P. Gollub, *Chaotic Dynamics: An Introduction* (Cambridge University, Cambridge, England, 1990), p. 120.

[14] A. Wolf, J. B. Swift, H. L. Swinney, and J. A. Vastano, "Determining Lyapunov exponents from a time series," Physica D **16**, 285–317 (1985).

[15] G. Benettin, L. Galgani, A. Giorgilli, and J. M. Strelcyn, "Lyapunov characteristic exponents for smooth dynamical systems and for Hamiltonian systems: A method for computing all of them," Meccanica **15**, 9–30 (1980).

[16] I. Shimada and T. Nagashima, "A numerical approach to ergodic problem of dissipative dynamical systems," Prog. Theor. Phys. **61**, 1605–1616 (1979).

DID GOD HAVE ANY CHOICE?

Let me turn to the question of whether the laws in any sense *have* to be what they are. Could the world have been otherwise? And if so, how has a selection been made? It has long been a dream of the unifiers that when we finally write down that elusive Theory of Everything in a single magnificent formula (that you can wear on your T-shirt, remember), this superlaw will be the only mathematically and logically self-consistent statement. Thus one reads the following in the book *Gravitation*, by Misner, Thorne, and Wheeler: "Some principle uniquely right and uniquely simple must, when one knows it, be also so compelling that it is clear the universe is built, and must be built, in such and such a way, and that it could not possibly be otherwise." It is this issue that I believe Einstein was referring to when he said that what really interested him was whether God had any choice in the construction of the world.

Paul Davies, in *Doing Science: The Reality Club, 2*, edited by John Brockman (Prentice-Hall, New York, 1991), pp. 63–64.